LEX LOCALIS-JOURNAL OF LOCAL SELF-GOVERNMENT
ISSN:1581-5374 E-ISSN:1855-363X
VOL. 24, NO. S1 (2026)

HYBRID ARITHMETIC PUZZLE OPTIMIZATION ALGORITHM BASED GRAPH NEURAL NETWORK FOR EARLY GASTRIC CANCER DIAGNOSIS AND CLASSIFICATION

S.Venkatesan

Professor, Department of Computer Science and Engineering Adhiyamaan College of Engineering (Autonomous) Hosur, selvamvenkatesan@gmail.com

ABSTRACT
In the worldwide, the most popular and one of the severe health issue is Gastric cancer (GC). The infection of Helicobacter pylori (H. pylori) commonly affect the chronic atrophic gastritis. To improve the patient survival, early diagnosis of GC is the challenging one because the diagnostic theories are did not explained and concretized with utmost of the existing computer-aided-diagnosis (CAD) model. Nowadays, the clinical management full spectrum quickly reshape via artificial intelligence (AI) systems to diagnose GC. This work focuses on hybrid optimization model with deep learning (DL) techniques for the effective diagnosis and classification of GC. Prior to the classification, the input data images are pre-processed using Wiener filter is to remove the noise from the GC image pixels and followed by Equilibrium Optimized k-means Clustering (EOk-C) performs segmentation of GC images thereby enhancing the challenges of irregular edges and mucosal features diversity. Adaptive Gray Level Co-occurrence Matrix (AGLCM) feature extraction is performed and the GC detection and classification is employed via Proposed Hybrid Arithmetic Puzzle Optimization Algorithm (HAPOA) with Graph Neural Network (GNN). MATLAB software simulates the proposed work and it is analyzed with various performance measures for the identification of proposed GC classification efficiency. The experimental analytical results disclose that the proposed GC classification performance is superior to other state-of-art techniques.

Keywords: Wiener filter, Equilibrium Optimized k-means Clustering, GLCM feature extraction, Hybrid Arithmetic Puzzle Optimization Algorithm based Graph Neural Network.

1. INTRODUCTION

Gastric cancer [1], also known as carcinoma of the stomach, is a cellular tumor that begins in the gastrointestinal tract. Just behind the vertebrae in the top center of the abdomen is where the intestines are located, food digestion and disintegration are assisted by the intestines,and any area of the digestive tract has a chance of developing cancerous cells. According to figures on global stomach-cancer prevalence provided in 2018 by the International Association for Investigate on Cancer, the global top investigating cancer organization, gastric cancer is among the three most common causes of cancer mortality and ranks as the fifth highest common disease in terms of new cases. The overall prevalence of stomach cancer worldwide in 2018, the largest occurrences are found in Eastern Asia and Eastern Europe, as can be demonstrated.

upper gastrointestinal (UGI) cancer [2], which includes stomach and throat cancers and is the third most prevalent reason for cancer-related mortality all over the world, continues to be an important global health concern. Around the world, cancer of the esophageal tract is placed sixth in terms of fatality and 7th in terms of prevalence, and its rate of recurrence after five years is still between 15% and 25%. Cancer of the esophageal junction [3] is less deadly than gastric cancer. It ranks as the third-leading worldwide factor in fatalities from cancer, around 783,000 humanity lost their lives to stomach malignancy in 2018.In nearly every country, less than 30% of patients with stomach cancer survive the disease for five years, the expected life probability of those diagnosed is greatly impacted by early identification of UGI disease. Since early malignancies have a 90% lifetime survival rate [4], UGI tumor detection is crucial for lowering patient death.

The majority of individuals with malignancies discover it in the initial or final stages, missing the ideal period of possibilities for the therapy [5], which lowers the individual's likelihood of survival. This is due to the limitations of physician expertise and the current cancer surveillance modern technology. Therefore, research into efficient cancer testing methods is important,as soon as feasible, treating stomach cancer that doesn't yet have spread to another organ,is the primary objective, treatment or an investigative technique may treat an illness. In some cases, combining chemotherapy [6] with surgery might raise the likelihood of a successful recovery. Since advanced cancer of the abdomen is not generally thought to be recoverable, the aim of medical care at that point is primarily to extend the lifespan of the individual and manage the illness's manifestations, conservative therapy includes various types of medical interventions, such as radiotherapy or immunotherapy.

Metastatic cancer [7], often known as cancer of the fourth stage, is an aggressive form,this often indicates that the tumor has migrated to adjacent organs or distant regions of the body from where it started. Humans can survive for many decades following therapy, even though this late stage of the disease needs specialist care,the subsequent examinations might be performed for a medical exam to identify gastrointestinal cancer. A biopsy [8] is the extraction of a tiny sample of material for microscopic analysis, merely a biopsy can definitively diagnose cancer; additional examinations can merely hint that it may be occurring. Fortunately, if the stomach has had extensive cancer damage, it may result in an obstruction that impairs the correct digestion of meals. Indications of a plugged stomach include sickness, throwing up, and the sensation too full after consuming. Surgery can also help you live a better life, for instance, it can eliminate discomfort brought on by tumors that are pushing on an internal organ or nerve, and it may be employed to get rid of a malignancy that is obstructing the gut. This work proposed a novel hybrid optimization with deep learning model for early gastric cancer diagnosis and classification. The below points summarizes the major contribution of this work.

- To use Wiener filter for noise removal from original image.
- To apply Equilibrium Optimized k-means Clustering (EOk-C) executing GC images segmentation.
- To extract Contrast, dissimilarity, correlation, homogeneity, energy, Fourier descriptor and entropy features by means of AGLCM.
- To perform GC classification such as normal, begin and malignant stages using HAPOA based GNN model.

The remaining sections of this paper is arranged as, Section 2 elaborates the existing research related to the classification of GC. After that, the proposed framework to detect and classify GC is outlined in section 3 followed by the experimental outcomes are discussed in Section 4. At last, section 5 concludes the paper.

2. RELATED WORK:

Lee et al. [9] have presented a deep convolutional neural network (DCNN) that distinguishes between tumors and non-cancers by using depth-wise recoverable transformations. After examining the system's ability to classify, they discovered that differentiation and supplementation improved the sorting system's accuracy since the used enhancement of the data mechanism avoided excessive fitting. Our emphasis on the characteristics of the tumor during retraining was made easier by the internist's qualified classification of the divided pictures as malignant or non-cancer. This approach could be crucial in determining the best course of action and making survival estimates while not a biopsy is being performed surgically. Hence, it is insufficient to use the dataset for larger networks.

Kosaraju et al. [10] have implemented a deep learning model based on multi-task Histopathology (DL-MH) that concurrently captures many scale sections for precise histopathology image interpretation. It catches intricate physical characteristics in both big and microscopic detector fields of a whole-slide picture and isolates two regions of identical dimension at both the highest and lowest resolution ranges. The performance of this method is increased than the other algorithms. Hence, the computational expenses are more.

Igarashi et al. [11] have described machine learning has prompted multiple state's gastrointestinal investigations into the autonomous location of intestines disorders and estimation of the extent of cancer infiltration. Retroactive information was gathered on 85,246 unprocessed upper gastrointestinal surgical pictures from 441 individuals with cancer of the gastric tract. Instruction and verification in the initial phase of the creation of the system are the database being gathered, which is necessary for an illness in each gastrointestinal tract under a comparable picture acquisition setting. It was discovered to be successful in data cleaning tasks for gathering EGD pictures. Nevertheless, the non-informative photos weren't utilized in this investigation.

Wang et al. [12] have demonstrated a deep learning method to predict from existing full slide H&E tarnished pictures of gastrointestinal cancer. According to the findings, cancer of the stomach pathologic pictures can show the state of the tumor mutation load. Additionally, without the need for additional tests or tools, the suggested technique may successfully diagnose individuals with elevated TMB after being trained on a sizable general database. Therefore, it is inadequate to administer to a larger group of cancer patients.

Li et al. [13] have evaluated the deep learning model for the use of data sets, image manipulation, and methods of classification in the detection of stomach cancer. To increase the size of the information set, investigators frequently employ techniques like movement, pruning, and dynamic interaction networks. Certain investigators processed each gastroscopic picture independently using threshold-based screening to eliminate unnecessary regions and flexible statistical equalization techniques to reduce illumination discoloration. The capacity to learn more picture characteristics will function superior. Thus, the complexity of the collected information sample and the kind of label are inadequate to categorize the outcomes in different ways.

Wang et al. [14] have developed a deep-learning approach with global average pooling (DL-GAP) in an endoscopy used to help diagnose. To create the rectal lesion historical data, we used colonoscopy photos from the Paediatric Hospital's digestive endoscopy department. Additionally, we used the recesses Learning-based image identification technique to categorize intestinal lesions. The settings of the model may be greatly simplified, which has a positive impact on the design's memory use and heaviness. Hence, it is challenging to guarantee the exceptional precision of lesion-competent detection.

Sun et al. [15] suggested a deep-learning method using radiometric to assess serosa infiltration in cancer of the gastric. An overall of 572 participants with stomach cancer was tested for detection and classification purposes. The surgical tissue samples served as the basis for pathological evaluation. A group of three specialists decided on the CT results that were used to create radionic signatures by extracting both traditional handmade attributes as well as advanced feature learning from multiple stages of CT pictures. It has strong specificity for diagnosis and is discriminative. Thus, manually segmenting the tumor using this method required a lengthy process.

Ding et al. [16] highlighted a semantic-level cancer-screening network (SCNET) a methodology for upper gastrointestinal (UGI) tumor identification that employs the semantic-level heterogeneous fusion of information. For boosting the efficacy of UGI tumor detection, the fundamental links between the geographic elements of UGI pictures and the linguistic

characteristics of written statements are found and combined throughout the three steps of data synthesis. This method considerably increases reliability and specificity for tumor detection using single- and multiple-modal samples. Additionally, the present strategy is built on extensive learning, which is not easily explicable.

3. PROPOSED FRAMEWORK:

The schematic model for proposed GC classification is sketched in Figure 1. Dataset provides the images and the original images are pre-processed via Wiener filter and the segmentation of GC using EOk-C model. The shape and GLCM features are extracted and GC classification is completed by hybrid optimization with deep learning. The following sub-section expands the outline of proposed work.

Fig 1: Schematic view of proposed work for GC classification

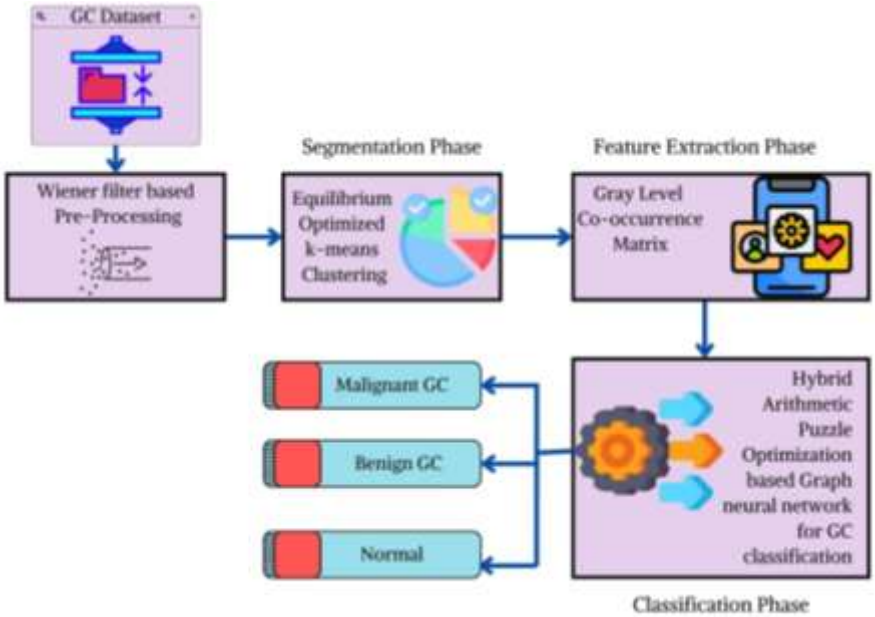

3.1 Pre-Processing:

Fed the original images into pre-processing using wiener filter (WF), which is the statistical model to neglect noise from every pixels. The best transaction among noise smoothing and inverse filtering is performed [17]. Overall noise is removed based on smoothing procedure in which the frequency domains are used by WF. Below formula represent the wiener filter.

$$wi(g_1,g_2)=\frac{h(g_1,g_2)\times s_a(g_1,g_2)}{\left|h(g_1,g_2)^2 s_a(g_1,g_2)+s_b(g_1,g_2)\right|} \quad (1)$$

The original and additive noise based on power spectra is $s_a(g_1,g_2)$ and $s_b(g_1,g_2)$ with the blurring filter is $h(g_1,g_2)$. The blur image inverting and additive noise removed from the histological images using WF.

3.2 Segmentation:

This work adopt Equilibrium Optimizer along with k-means clustering model, which is named as Equilibrium Optimized k-means Clustering (EOk-C) to segment the GC regions. The step by step process is elaborated as below,

3.2.1 The K-Means Clustering Approach

During image dta point partitioning, improve the given representative vectors set mapping. From the histological images, the GC afffected regions are segmented from the helathy pixels using k-means clustering model. Clsuter the M image instances into k pixel clsuters [18]. Randomly select the initial centroids. Next to initialization, start the itterative procedures. Update the pixel centriods after defining clusters. Below formula calculates the centriods (C_j) in which one cluster is assigned based on the image instances.

$$C_j = \frac{1}{\left|R_j\right|}\sum_{Y_j \in R_j} Y_i \qquad (2)$$

Where, $j = 1,2,...,k$ and the j[th] cluter with the nuber of intances are $\left|R_j\right|$. While reducing the sum of squared Eucledian distance among the image centriods and instances within every instances, the optimiation issue defines k-means model.

$$Fitness = \sum_{j=1}^{k}\sum_{Y_j \in R_j} D\left(C_j, Y_i\right) \qquad (3)$$

Euclidean distance among two image pixels are $D\left(C_j, Y_i\right)$. The disjoint cliuters are pixels divides the image (instance) during GC segmentaion. Define the pixel diatances while using k-means clustering. The image intenity level and pixel position defines the distances. Differences among intensity level defines the two pixel distances. The k-means clsutering met the challenges of health background of mucosa, mucosal feature diversity and unable to solve edge irrregularity. Therefore, the Equilibrium Optimizer (EO) model is selected and combined with k-means clustering for the accurate and improved segmentation of GC.

3.2.2 Equilibrium Optimizer

The control volume dynamic mass balance inspires the Equilibrium Optimizer (EO) model. To conserve mas entering, physics provided the equation of balance mass.

$$U\frac{dM}{dt} = qM_{sim} - qM + H \qquad (4)$$

The control volume of the particle and it concentration is U and M with the rate of flow of volume is q [19]. At the state of equilibrium without generations, the control volume within the particle concentration is M_{sim}. Reach the steady state of equilibrium (sim) at $U\frac{dM}{dt} = 0$.

Equation (4) is rearranged as,

$$\frac{dM}{\delta M_{sim} - \delta M + \frac{G}{\nabla}} = dt \qquad (5)$$

$$M = M_{sim} + \left(M_0 - M_{sim}\right)H + \frac{G}{\delta \nabla U}\left(1 - H\right) \qquad (6)$$

$$H = \exp\left[-\delta\left(1 - t_0\right)\right] \qquad (7)$$

Both concentration interval and initial start time are M_0 and t_0.

❖ **Initialize candidate solution and term of exponential:**

When the averge support in exploittaion, the search space is explored with four best particles in which the below eexpression explins equlibrium pool vector [20].

$$\vec{M}_{sim,\,pool} = \vec{M}_{sim_1}, \vec{M}_{sim_2}, \vec{M}_{sim_3}, \vec{M}_{sim_4}, \vec{M}_{sim_{avergae}} \qquad (8)$$

Radom selection is updated and adopting every particle in each iteration. Similarly, all candidate solutions are updated at the time. The EO algorithm explortaion and exploitation is balanced using the vital role of exponential term (H). Interval of [0, 1] is for random vector ranges δ . The number of iteration minimizing the iterative function t.

$$\overrightarrow{H} = e^{-\vec{\delta}(t-t_0)} \quad (9)$$

$$t = \left(1 - \frac{iteration}{Maximum\ iteration}\right) \quad (10)$$

$$\dot{t}_0 = \frac{1}{\delta}\ln\left(-b\ sign\left(\vec{R} - 0.5\right)\left[1 - e^{-\vec{\delta}t}\right]\right) + t \quad (11)$$

Where, the constant is b to control the exploitation and exploration stage.

❖ **Rate of Generation:**

The exploitation stage is improved to demonstrate the accurate solutions enabled via generation rate (gen). The decay constant is k with the initial value is $\overrightarrow{gen}_0$.

$$\overrightarrow{gen} = \overrightarrow{gen}_0 e^{-\vec{k}(t-t_0)} \quad (12)$$

$$\overrightarrow{gen} = \begin{cases} 0.5R_1, & R_2 \geq P \\ 0, & R_2 < P \end{cases} \quad (13)$$

During the updating process, the generation term probability is P. Better exploitation and exploration is accomplished via role of generation probability in which the EO rule updating is given as,

$$\overrightarrow{M} = \overrightarrow{M}_{sim} + \left(\overrightarrow{M} - \overrightarrow{M}_{sim}\right)\overrightarrow{H} + \frac{\overrightarrow{H}}{\delta U}\left(1 - \overrightarrow{H}\right) \quad (14)$$

The considered unit is U. The optimal point is determined with global search.

3.2.3 GC Segmentation Using (EOk-C)

This study embrace EO with k-means clustering (EOk-C) model to find best centroids thereby enhancing segmentation performance of GC. The k-means algorithm result is based on the initial solution of EO with its search ability and better rate of convergences. The k-means algorithm with one iteration improves the achieved solutions in every generation [21]. The best threshold value of an image based on histogram is identified using EO fitness function. Overall inter-cluster distance, determine the segmentation (clustering) performance. To reduce intra-cluster distance, distance maximization equal to it the major concentration. Based on L-level of image segmentation, the image intensity iwith the number of pixel is represented as $Y(j)$.

$$Fit(T) = \sum_{j=0}^{k} W_j \beta_j^2 \quad (15)$$

The proposed EOk-C receives the cluster centers related to the image threshold value is determined using fitness function of EO. Inside each cluster, higher intensity level of pixel determines the threshold values after allocating instances to relevant clusters. The threshold criteria is achieved to sort the obtained values and the proposed EOk-C model obtains the solution of quality measure in which it optimally segmenting GC from the original image background. The GC segmentation using EOk-C pseudocode is outlined in algorithm 1.

Algorithm 1:Pseudocode for GC segmentation using EOk-C approach
Initialization of number of clusters, balance mass, with current and maximum number of

iterations
Sort and determine the threshold value for every solution
Calculate the fitness function
Compute concentration interval M_0 and initial start time t_0
Determine the equlibrium pool vector
Update equation (2) to calculating the centriods (C_j)
For j=1:m
If $R_2 \geq P$
Equation (13) update the generation rate
The fitness value is calculated using equation (15)
Sort and find the threshold values
EndIf
Update the generation probability to balance exploration and exploitation
End For
Set the best one cluster as the segmented region of CG regarding the ranking of solutions
Repeat
To obtain maximum iteration met

3.3 Feature Extraction:

The gray scale matrix image pixel shape is analyzed as the evaluation model called Gray Level Co-occurrence Matrix (GLCM). GLCM model extract the features from the segmented images. Calculate the feature vector based on the classifier performances. Several classes signified with the features are extracted by examining image features [22]. To identify the severity stages of GC, use shape, intensity and texture based approaches based on GLCM. The lesion boundaries describe the shape features in which the gray level spatial distributions are texture features in segmented GC images. The shape based feature uses Fourier descriptor, intensity based features are extracted via entropy and GLCM extract the texture features in which the amalgamation of these features are called as adaptive GLCM (AGLCM). Texture feature extraction in terms of GLCM in which the gray pixel level distribution resulted. Both neighbor and reference pixels computes the spatial distribution among two pixels [23].

The neighbor pixel frequency is represented using co-occurrence matrix in which the distance separate it. The distance with eight kind of directions with respect to various angles calculates the occurrences probability. Contrast, dissimilarity, correlation, homogeneity, energy are the features calculated from co-occurrence matrix. Image variations are calculated using homogeneity features in which the textual uniformity are computed by means of energy features. The neighboring pixel's linear dependency is indicated using GLCM correlation. Spatial frequency of image calculated using contrast features and the distance among a pair of pixels are computed with the help of dissimilarity features.

3.4 GC detection and Classification:

This section extends the classification of GC using the proposed novel Hybrid Arithmetic Puzzle Optimization algorithm (HAPOA) based Graph Neural Network (GNN), which utilizes the Puzzle Optimization algorithm and Arithmetic Optimization Algorithm for the tuning of hyper parameters. The concise of proposed work is framed in the below sections.

3.4.1 Puzzle Optimization Algorithm (POA)

The puzzle optimization algorithm relies on the process involved in puzzle game. The best member from the population is chosen and is used for solving the puzzle [24]. The identification of the problems is must to interpret the mathematical expression,

$$M = \begin{bmatrix} M_1 \\ \vdots \\ M_j \\ \vdots \\ M_Y \end{bmatrix}_{Y\times n} = \begin{bmatrix} M_1 & \cdots & M_{1,D} & \cdots & M_{1,n} \\ \vdots & \ddots & \vdots & \iddots & \vdots \\ M_{j,1} & \cdots & M_{j,D} & \cdots & M_{j,n} \\ \vdots & \iddots & \vdots & \ddots & \vdots \\ M_{Y,1} & \cdots & M_{N,D} & \cdots & M_{Y,n} \end{bmatrix}_{Y\times n} \quad (16)$$

The total number of population in the puzzle or total number of pixels in the images is taken as Y and the j[th] pixel in the gastric cancer image is M_j and the variables of problem is implied as n. the dimensionality of the search space is D. the objective function of the images are interpreted as,

$$F = \begin{bmatrix} Ob_1 \\ \vdots \\ Ob_j \\ \vdots \\ Ob_Y \end{bmatrix}_{Y\times 1} = \begin{bmatrix} F(M_1) \\ \vdots \\ F(M_j) \\ \vdots \\ F(M_Y) \end{bmatrix}_{Y\times n} \quad (17)$$

The vector value of respective objective function (Ob_i) is F. henceforth the best member from the total pixel is determined as,

$$Bes = M_i, Ob_i = Min(F) \quad (18)$$

The minimal objective function $Min(F)$ is evaluated using the M_i *and* Ob_i for the ith pixel. The pixel of every image Y_j^{new} are updated using the control of other images. Based on the pixels, every member finishes the puzzle as shown below,

$$M_j^{new} = M_i + Rand \times DM_j \quad (19)$$

$$M_j = \begin{cases} M_j^{new}, & F_j^{new} < F_j \\ M_j, & Otherwise \end{cases} \quad (20)$$

The total number of pixels in the gastric cancer images is taken as Y_r. The maximum number of iteration is T and the current iteration is t and is outlined as,

$$Y_r = Round\left(0.5 \times \left(1 - \frac{t}{T}\right) \times Y\right) \quad (21)$$

Based on the iterations the new populations of images are determined and the optimal solution is attained with the quasi-best solution approach.

3.4.2 Arithmetic Optimization Algorithm

This optimization relies on the arithmetic operators used for solving the issues occur during the arithmetic operations. The initialization of AOA is based on setting the candidate solutions as shown in matrix below. These are created randomly with the best-obtained solution.

$$G=\begin{bmatrix} g_{1,1} & \cdots & \cdots & g_{1,j} & g_{1,n-1} & g_{1,n} \\ g_{2,1} & \cdots & \cdots & g_{2,j} & \cdots & g_{2,n} \\ \cdots & \cdots & \cdots & \cdots & \cdots & \cdots \\ \vdots & \vdots & \vdots & \vdots & \vdots & \vdots \\ g_{N-1,1} & \cdots & \cdots & g_{N-1,j} & \cdots & g_{N-1,n} \\ g_{N,1} & \cdots & \cdots & g_{N,j} & g_{N,n-1} & g_{N,n} \end{bmatrix} \quad (22)$$

The searching phase can begins with the calculation of Math Optimizer Accelerated function (MOA) as below,

$$MOA(c\_iter)=Minimum+c\_iter\times\left(\frac{Maximum-Minimum}{M\_iter}\right) \quad (23)$$

The function value when the iteration is t is evaluated with eqn. (23). The current iteration is implied as c_iter. The accelerated function with maximum and minimum values are denoted as $Maximum$ and $Minimum$respectively [25]. The maximum number of iteration is taken as M_iter.

(I) Exploration Stage

This stage finds the better solution with two operators namely division D and multiplication M as shown in eqn. (24). It also used to update the location of the pixels in the image and is formulated as,

$$g_{i,j}(c\_iter+1)=\begin{cases} Bes(g_j)\div(MOP+\in)\times\left(\left(TU_j-TL_j\right)\times\delta+TL_j\right), & z_2<0.5 \\ Bes(g_j)\times MOP\times\left(\left(TU_j-TL_j\right)\times\delta+TL_j\right), & otherwise \end{cases} \quad (24)$$

The i[th] solution is $g_i(c_iter+1)$of the next iteration and the iteration of jth location for the ith solution of the ongoing iteration is $g_{i,j}(c\_iter)$. The best acquired solution for the jth location is $Bes(g_j)$. The integer number that is small in size is $\in$. The lower and upper constraints are TL_j and TU_jcorrespondingly for the j[th] location. The searching can be improved by the control parameter δ with the pre-defined value 0.5. The Math optimizer probability (MOP) of the C_iter is formulated as shown below,

$$MOP(c\_iter)=1-\frac{c\_iter^{\frac{1}{\chi}}}{M-iter^{\frac{1}{\chi}}} \quad (25)$$

(Ii) Exploitation Stage

The sensitive factor χ is used to define the iteration accuracy and taken as 5. The exploitation strategy can be defined as,

$$g_{i,j}\left(c\_iter+1\right)=\begin{cases} Bes(g_j)-MOP\times\left(\left(TU_j-TL_j\right)\times\delta+TL_j\right), & z3<0.5 \\ Bes(g_j)+MOP\times\left(\left(TU_j-TL_j\right)\times\delta+TL\right), & otherwise \end{cases} \quad (26)$$

The exploitation stage is used to avoid falling to the local minima.

3.4.3 Hybrid Arithmetic Puzzle Optimization Algorithm (HAPOA)

Single optimization algorithms have low diversity and not used for sharing the data within the taken pixel population of the gastric cancer images. Meanwhile, the AO has some issues like

easily fall for local solutions and reduced convergence speed. Besides, the adopted PO has better searching capacity in the search space. To tackle the issues faced in the AO and utilizes the full usage of PO we presented a hybrid approach known as HAPOA. The combination of both algorithms escalates the population diversity with the useful information [26]. Moreover, the valuable solutions can be evaluated in a very low time and improves the diversity. For further enhancement, the Brownian mutation and Levy flights are merged with the HAPOA. For improving the exploration phase Levy flight is used and exploitation phase is enhanced with the Brownian mutation. The modified exploration phase of eqn. (24) is given as,

$$g_{i,j}(c\_iter+1)=\begin{cases} Bes(g_j)\times Levy(j)\div(MOP+\in)\times\left(\left(TU_j-TL_j\right)\times\delta+TL_j\right), & z_2<0.5 \\ Bes(g_j)\times Levy(j)\times MOP\times\left(\left(TU_j-TL_j\right)\times\delta+TL_j\right), & Otherwise \end{cases} \quad (27)$$

The schematic overlay of proposed HAPOA is outlined in figure 2.

Fig 2: Schematic overlay of proposed HAPOA

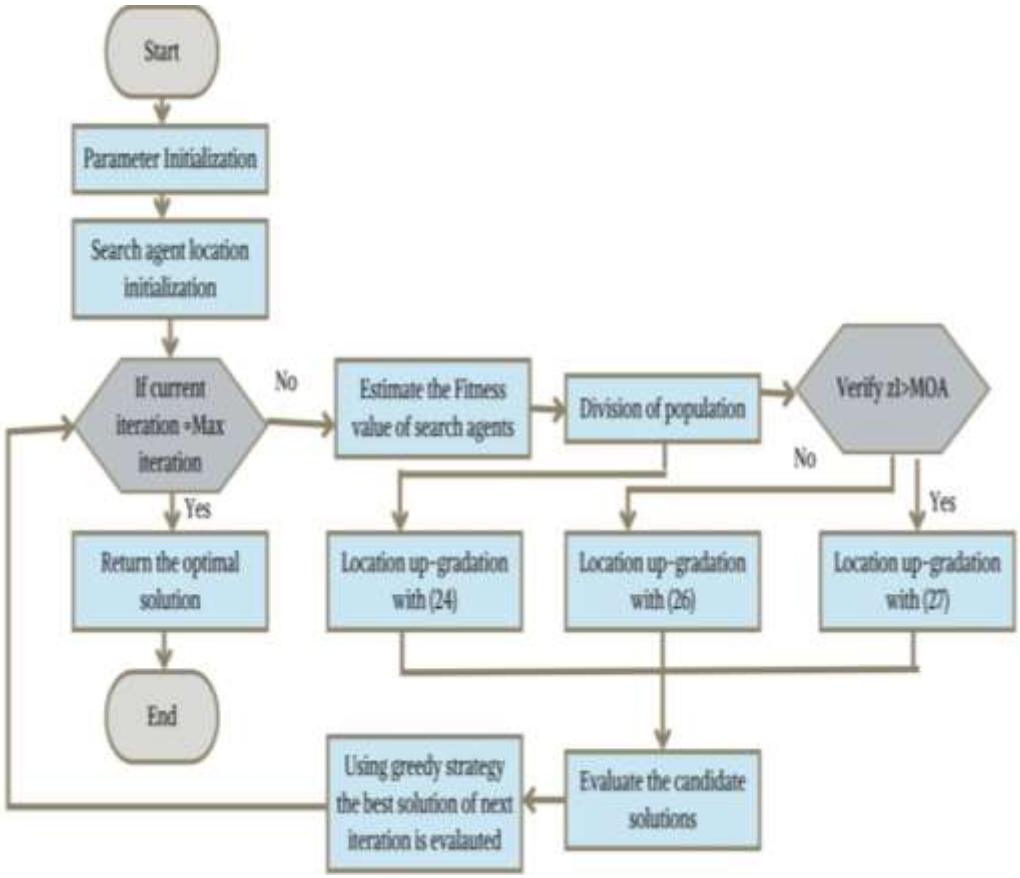

3.4.4 Computational Complexity of HAPOA

The initialization stages of HAPOA arbitrarily select the search agents and the computational complexity of this stage is $O(N\times D)$, the total dimensionality of the search space is D and total number of population is N. the complexity of total iteration while estimating the fitness function is $O(N\times D\times T)$. The computational complexity of adding the Levy flight, Brownian mutation, AOA, and PO are $O(3\times N\times D\times T)$. Finally, the computational complexity of the proposed HAPOA is $O(N\times D\times T)$.

3.4.5 Graph Neural Network

The GNN does not depend on the object labels and aims to predict the labels accurately with the succor of learning object representation persuasively. The learning of object representation is effectuated with the encoding of local graph framework and the features of attributes [27]. The full framework of GNN is framed in figure 3. Meanwhile, the training of whole structure takes place in an end-to-end structure. The joint distributions of labels of GNN are factorized fully as:

$$D(Bw|Aw) = \prod_{n \in W} D\left(B_n|Aw\right) \tag{28}$$

The posterior label distribution of the unlabeled objects is termed as $D(Bw|Aw)$ and for each object the label distribution is $D\left(B_n|Aw\right)$ and is deemed for n objects. The GNN prediction for the taken n objects from the gastric cancer image is formulated as follows,

$$l = h(Aw, F)\ D(B_n|Aw) = Cat\left(B_n|soft\max(Vl_n)\right) \tag{29}$$

All objects are determined as $l \in \Re^{|w| \times g}$ and the nth object is determined as $l \in \Re^{g}$. Meanwhile the linear transformation matrix is $V \in \Re^{K \times g}$ with the label classes κ and the dimensionality determination as g. the categorical distributions is determined as Cat. For learning purpose of object the l is used. For updating the l each current value and neighbor of the image pixels are used from the gastric cancer images from the patients. For updating we have utilized graph attention layer and multiple layers are updated. The object determination obtained after the final process, the values are forwarded to the softmax classifier for the prediction of label.

Fig 3: Full Framework of proposed GNN

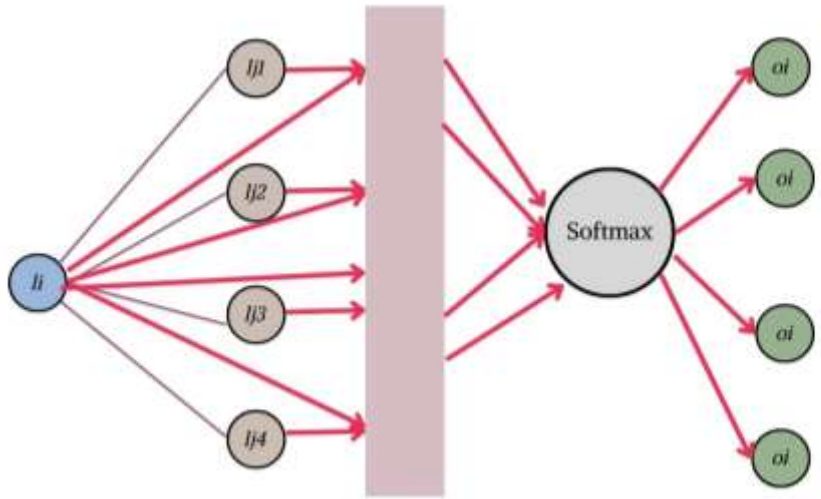

3.4.6 Proposed HAPOA based GNN for the GC classification

The selection of best features from the gastric cancer images that are extracted above can be enhanced with the proposed HAPOA-GNN approach for the classification of images as Malignant, Benign, and normal. The classification of gastric cancer can be obtained from the set of optimal features with the help of AOA by tuning the hyper parameters of GNN. The features that are ignored by the AOA are forwarded to the PO for reformation [28]. The population of PO is generated using the ignored features and the location up-gradation is

effectuated with the non-fit individuals. The features that are selected by the PO are pushed to the AOA as a new population. The fitness functions are evaluated to increase the classification accuracy of GNN. The roadmap of proposed HAPOA based GNN is framed in figure 4.

Fig 4: Roadmap of proposed HAPOA based GNN for the GC classification

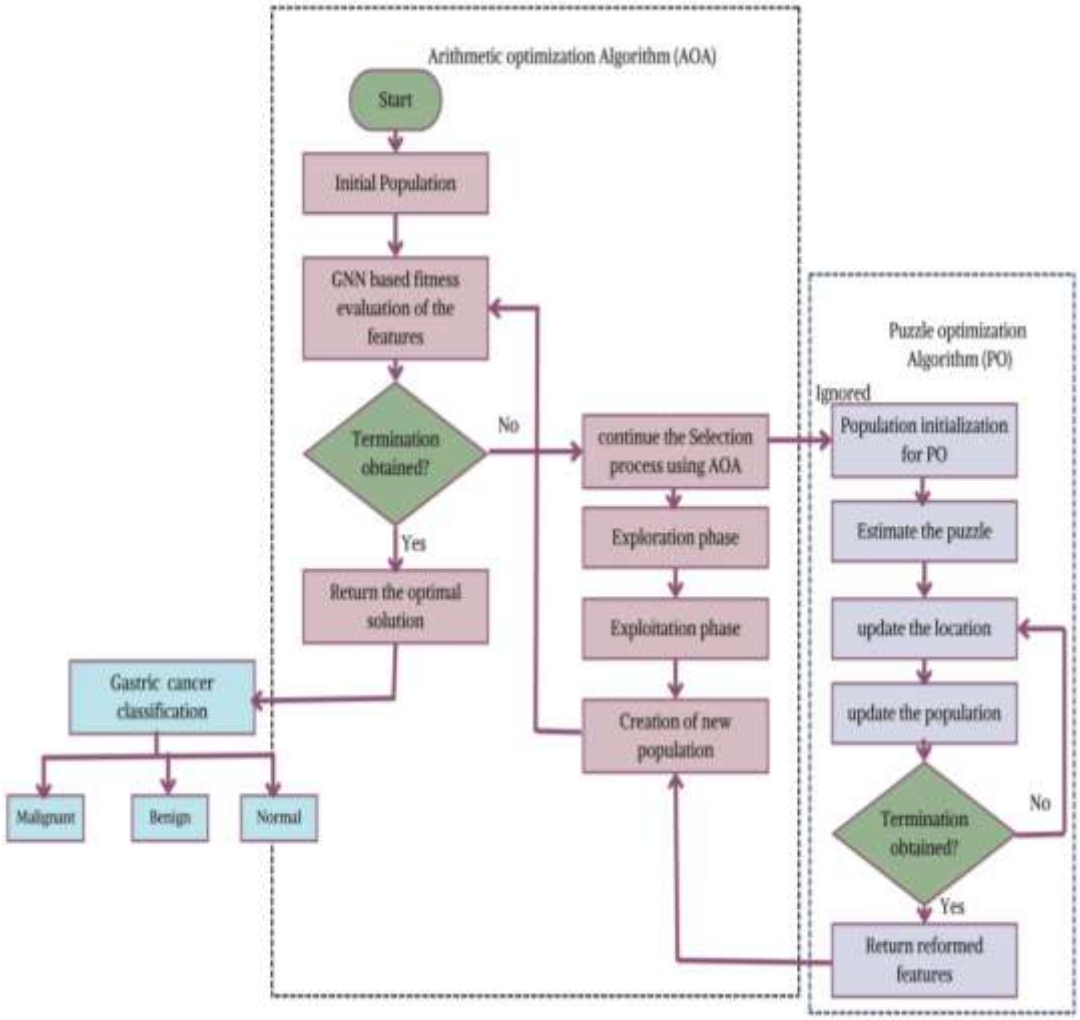

4. Experimental Results and Discussions:

At 4GHz8GB RAM, Windows 10 Professional OS with the Intel ® CoreTM i5-9700K CPU platform test the proposed GC classification performance, which is simulated under the environment of MATLAB. The population size of 100 with 300 number of iterations selected.

4.1 Dataset Explanation:

During an examination, the dataset image gathered from Fujita Health University Hospital endoscopy center. A total of 1208 images gathered. Among this, healthy images are 42 with begin GC images are 533 and the remaining images of 637 are malignant GC. Sample images of GC with segmented outputs are illustrated in Figure 5. From this, the first row represent the sample images and the second row represent the segmented result of respective original images.

Fig 5: Sample images of GC with segmented outputs

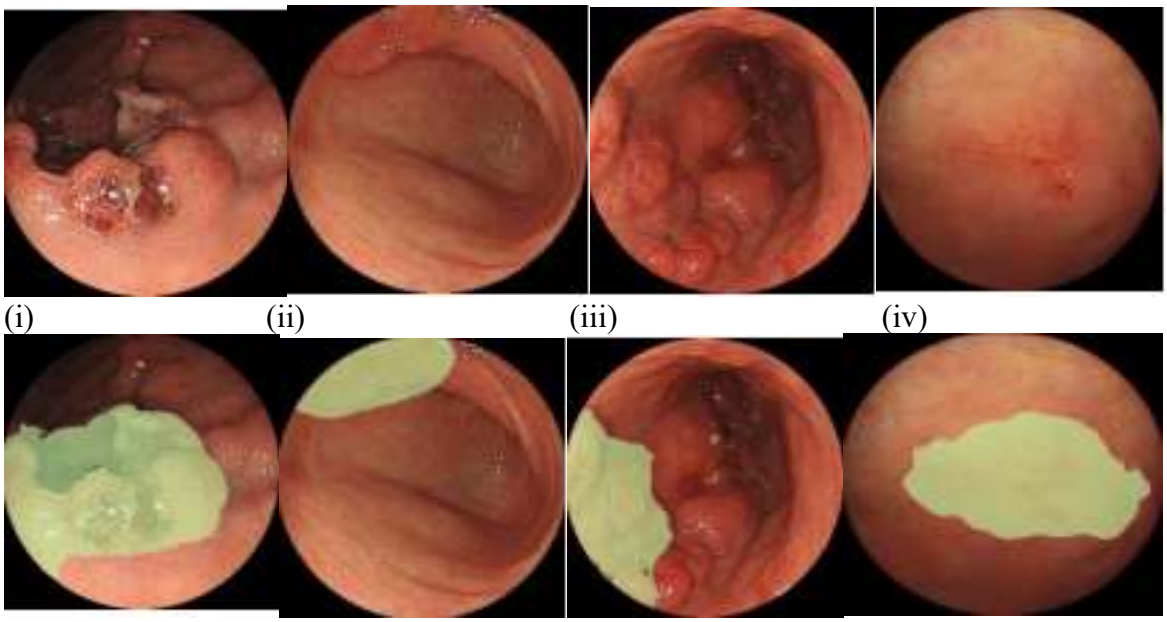

4.2 Evaluation Measures:

The statistical metrics such as structural similarity index measure (SSIM), peak signal to noise ratio (PSNR), mean square error (MSE) and normalized root mean square error (NRMSE) to measure the segmented image outcomes. The similarity among original and GC segmented image performance is described using SSIM. SSIM values of two similar images tends to the ranges [-1, 1].

$$SSIM = \frac{\left(2\chi_e\chi_f + D_1\right)\left(2\lambda_{ef} + D_2\right)}{\left(\chi_e^2 + \chi_f^2 + D_1\right)\left(\lambda_e^2 + \lambda_f^2 + D_2\right)} \quad (30)$$

Mean values of both segmented (f) and original (e) images are χ_f and χ_e with its covariance are λ_f^2 and λ_e^2. The stabilizing division variables are D_1 and D_2. NRMSE is explained below.

$$NRMSE = \sqrt{\frac{\sum_{j=1}^{E}\sum_{k=1}^{F}\left(y(j,k) - z(j,k)\right)^2}{\sum_{j=1}^{E}\sum_{k=1}^{F}\left(x(j,k)\right)^2}} \quad (31)$$

Where, $E \times F$ is the image. At position (j, k), the original and segmented image pixel intensity is $y(j,k)$ and $z(j,k)$. When the NRMSE of two identical images to zero when the smaller values for NRMSE is best. PSNR is calculated as below and the unit is dB. The maximum intensity value is $Max1$.

$$PSNR = 10\log_{10}\left(\frac{Max1^2}{MSE}\right) \quad (32)$$

The processed outputs based on various techniques are outlined in Table 1. Here, the methods namely histogram equalization (HE) [29], adaptive histogram equalization (AHE) [30], contrast-limited adaptive histogram equalization (CLAHE) [31] and median filter (Proposed) to show the efficiency of pre-processed Image with respect to the measures like MSE and

PSNR. This investigation discloses that median filter outperformed minimum of 6.75 MSE and maximum of 44.45 than other pre-processing techniques such as HE, AHE and CLAHE.

Table 1: Pre-processed results of various methods

Techniques	PSNR [dB]
HE	20.31
AHE	19.32
CLAHE	30.32
Median filter (Proposed)	44.45

Table 2 explains the feature extraction results based on various features. The varying angle of 0^0, 45^0, 90^0 and 135^0 with various extracted features from GC image with its result is displayed.

Table 2: Feature extraction results based on various features

Name of the features	0^0	45^0	90^0	135^0
Dissimilarity	32.075	27.848	13.586	25.906
Homogeneity	0.378	0.408	0.529	0.410
Energy	0.349	0.384	0.480	0.384
Contrast	3162.32	3834.56	1024.54	2348.43
Correlation	0.602	0.584	0.889	0.661
Mean of Fourier descriptor	141.192			
Entropy	27.267			

Figure 6 oulines the comparative result of SSIM. The comparison of SSIM is computed based on the methods such as Otsu method, C-means clustering, k-means clustering and proposed EOc-M methods. There are 300 iterations are selected in which the result of 82%, 85%, 82% and 96.7% of SSIM outputs in terms of Otsu method, C-means clustering, k-means clustering and proposed EOc-M methods at 300th iterations. Anyway, by comparing the other methods, the proposed technique complete grater SSIM results.

Fig 6: Comparison evaluation for SSIM

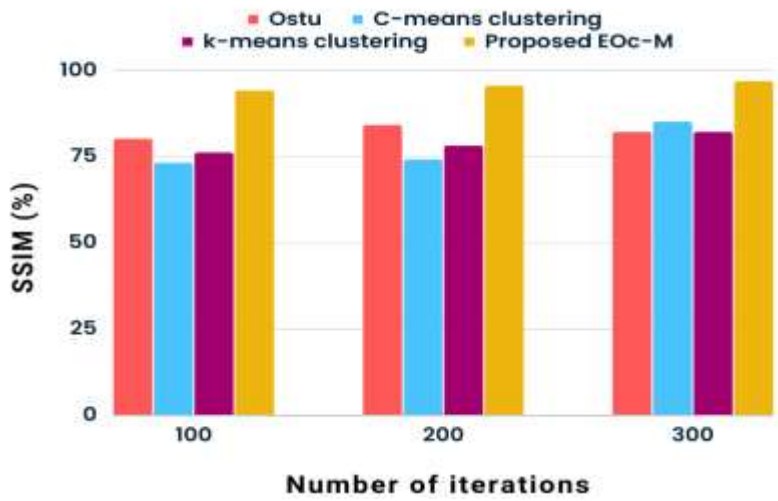

The NRMSE results are plotted in Figure 7. The NRMSE comparison is calculated using the techniques namely Ostu method, C-means clustering, k-means clustering and proposed EOc-

M methods. From this graphical analysis, we have obtained the result of 0.69%, 0.72%, 0.67% and 0.43% of NRMSE outputs in terms of Ostu method, C-means clustering, k-means clustering and proposed EOc-M methods at 300th iterations. The NRMSE of proposed method takes minimum results to compare with other techniques.

Fig 7: Comparison evaluation for NRMSE

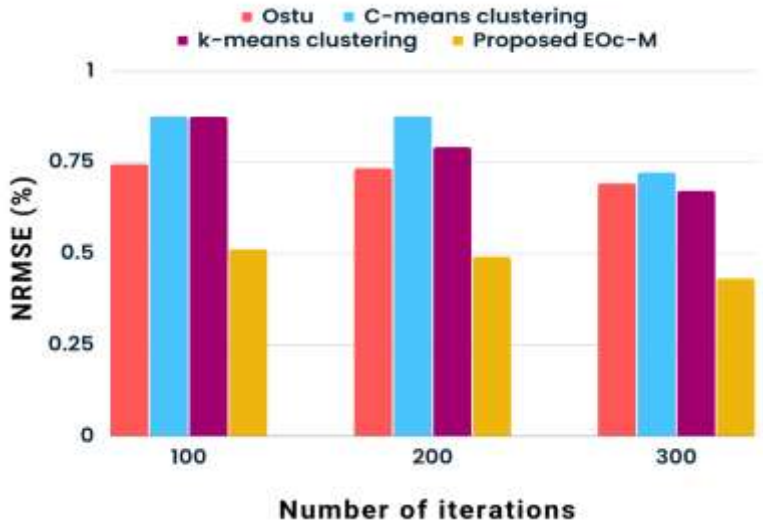

The GC classification is the predominant step in the detection of GC cancer for the early prediction to avoid fatality. The proposed approach efficiently classifies the GC from the taken images. However, to ensure this, it is necessary to compare the proposed approach with state-of-art works such as DCNN, DL-MH, DL-GAP, and SCNET. For that we have taken the statistical parameters such as Accuracy, Precision, Recall, and computational time. Prior to the comparison we have presented the elucidation of the statistical parameters as below.

- **Accuracy: It** is used to describe the efficiency of the model that is how accurately the model classifies the GC images as normal, malignant, and benign. It is interpreted as,

$$A = \frac{Exactly\,classified\,GC\,\mathrm{Im}\,age\,samples}{Total\,number\,of\,samples} \qquad (33)$$

- **Precision:** It is described as how effectively the proposed model identifies the true positives and is interpreted as,

$$P = \frac{TPV}{TPV + FPV} \qquad (34)$$

Here, TPV is the true positive value; FPV is the false positive value.

- **Recall:** It is described as the proportion of true positive predicted values and the total predicted false negative and true positive values. it can be interpreted as,

$$R = \frac{TPV}{TPV + FNV} \qquad (35)$$

FNV is the false negative value that is predicted well.

- **Computational Time:** It is described as the time taken by the system to finish the total classification approach. It is mostly measured in seconds.

Fig 8: Analogous of proposed and state-of-art works in terms of accuracy

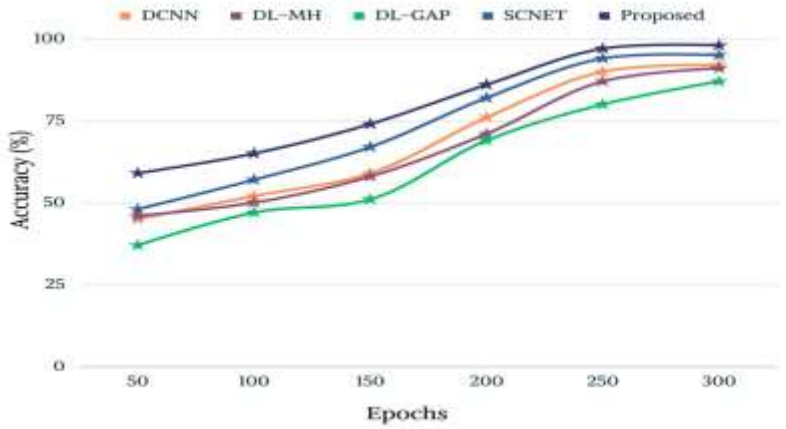

The Analogous of proposed work and state-of-art works such as DCNN, DL-MH, DL-GAP, and SCNET in terms of accuracy of GC classification is outlined in figure 8. The figure illustrates the classification accuracy of proposed approach is 98% after the epoch of 300. At starting the accuracy is lower and the increasing the increasing epoch. This because the GNN effectively chooses the features, that are extracted from the previous section and classifies the GC as normal, Malignant and Benign. The main characteristics of GNN are it trains the labels in an end to end passion and hence the classification made easier. The inclusion of softmax layer in GNN also enhances the classification accuracy. Meanwhile, the proposed HAPOA effectively improves the hyper-parameter tuning to prevent the overfitting issues as well as the falling for unmatched features. Thus the classification accuracy of proposed approach is higher for all the epochs than the other works. The accuracies of state-of-art works such as DCNN, DL-MH, DL-GAP, and SCNET at epoch 300 are given as 92%, 91%, 87% and 95% respectively.

Fig 9: Analogous of proposed and state-of-art works in terms of Precision

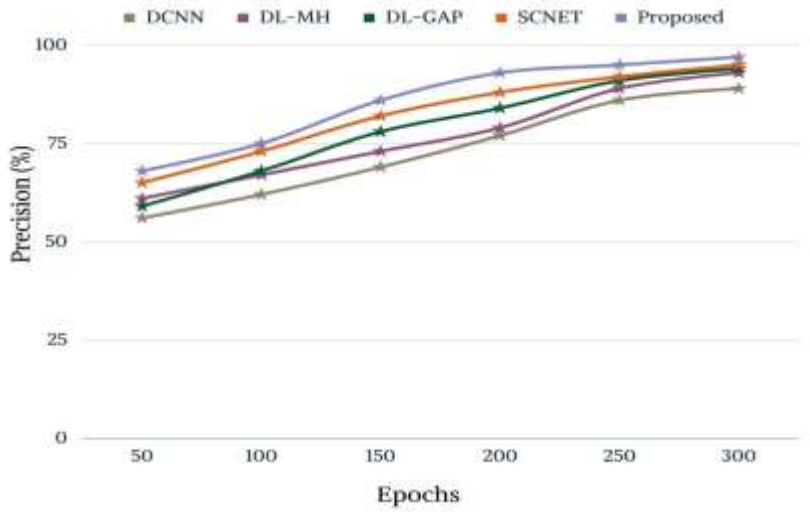

The precision value based graphical representation is visualized in figure 9. It shows the analogous of proposed and state-of-art works such as DCNN, DL-MH, DL-GAP, and SCNET. We have taken 300 epochs and after 300 epochs the results become constant and we halted the process. At 300^{th} epochs the proposed approach provides precision of 97% which is greater than all the other approaches. The effective prediction of GC as normal, Malignant and Benign improves the precision value too. From epoch 50 itself the proposed approach

shows better outcome than the proposed approach. Since the GNN does not depend on the object labeling the classification become easier and also the HAPOA also enhances the classification prediction. At 300th epoch the state-of-art works such as DCNN, DL-MH, DL-GAP, and SCNET show the precision of 89%, 93%, 94%, and 95% respectively.

Fig 10: Analogous of proposed and state-of-art works in terms of Recall

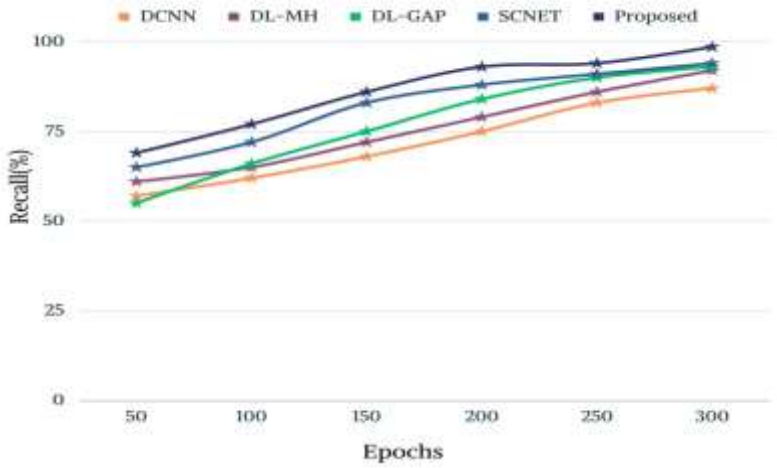

Visualization of analogous study of proposed and state-of-art works such as DCNN, DL-MH, DL-GAP, and SCNET based on recall is shown in figure 10. As mentioned above for this recall also we have conducted 300 epochs, the reason of conducting 300 epochs is that the statistical parameters increase their value with increasing epochs and after reaching the bias point the values get constant. In our work, after 300 epochs the value becomes constant and the recall of proposed approach is 98.56%. Meanwhile, the state-of-art works such as DCNN, DL-MH, DL-GAP, and SCNET provide recall value of 87%, 92%, 93%, and 94% respectively lower than the proposed approach at 300th epochs.

The computational time of proposed and state-of-art works such as DCNN, DL-MH, DL-GAP, and SCNET in second is listed in table 3. The adoption of effective techniques decreases the time utilization. The time taken to complete the entire process by our proposed approach is lower than the other state-of-art works. The EOk-clustering optimizes the segmentation process and proposed HAPOA also optimizes the process and the time utilization of proposed approach is lower with the value of 87 seconds. Meanwhile, other approaches such as DCNN, DL-MH, DL-GAP, and SCNET utilized time of 256s, 378s, 198s, and 135 s respectively as mentioned in the table 3.

Table 2: Analogous of proposed and state-of-art works in terms of Computational time

Methods	Computational time (s)
DCNN	256
DL-MH	378
DL-GAP	198
SCNET	135
Proposed	87

5. CONCLUSION:

In a nutshell, the proposed work is classify the GC images into normal, Malignant, and benign. For that we have proposed an innovative approach known as HAPOA based GNN approach. For effective classification the work conducted several steps such as preprocessing,

segmentation, and feature extraction prior to the classification. Pre-processing step has been effectuated with the Wiener filter to format the images in a required form. The second step segmentation has been effectuated with the proposed novel EOk-C which segments the GC images and overcame the challenges faced with irregular edges. The feature extraction has been conducted with the GLCM for the effective feature selection. With the succor of these features the classification of images has been performed with the proposed approach. Experiments were conducted and compared the results of proposed approach with state-of-art works such as DCNN, DL-MH, DL-GAP, and SCNET. The proposed approach surpassed all the other approaches with the accuracy of 98%, precision of 97%, recall of 98.56% and with the mitigation of computational time of 87s.

REFERENCES:

[1] Meng, L., Dong, D., Chen, X., Fang, M., Wang, R., Li, J., Liu, Z. and Tian, J., 2020. 2D and 3D CT radiomic features performance comparison in characterization of gastric cancer: a multi-center study. IEEE journal of biomedical and health informatics, 25(3), pp.755-763.

[2] Campisano, F., Remirez, A.A., Landewee, C.A., Caló, S., Obstein, K.L., Webster, R.J. and Valdastri, P., 2020. Teleoperation and contact detection of a waterjet-actuated soft continuum manipulator for low-cost gastroscopy. IEEE Robotics and Automation Letters, 5(4), pp.6427-6434.

[3] Amuthan, N., Velrajkumar, P., Sivakumar, N. and Jarin, T., 2023. IOT based adjustment mechanism for direct reference model adaptive IMC to support voltage sag in DFIG wind farm. Measurement: Sensors, 27, p.100809.

[4] Vijay, M.M., Sunil, J., Vincy, V.A.G., IjazKhan, M., Abdullaev, S.S., Eldin, S.M., Govindan, V., Ahmad, H. and Askar, S., 2023. Underwater wireless sensor network-based multihop data transmission using hybrid cat cheetah optimization algorithm. Scientific Reports, 13(1), p.10810.

[5] Noaro, G., Cappon, G., Vettoretti, M., Sparacino, G., Del Favero, S. and Facchinetti, A., 2020. Machine-learning based model to improve insulin bolus calculation in type 1 diabetes therapy. IEEE Transactions on Biomedical Engineering, 68(1), pp.247-255.

[6] Byra, M., Dobruch-Sobczak, K., Klimonda, Z., Piotrzkowska-Wroblewska, H. and Litniewski, J., 2020. Early prediction of response to neoadjuvant chemotherapy in breast cancer sonography using Siamese convolutional neural networks. IEEE Journal of Biomedical and Health Informatics, 25(3), pp.797-805.

[7] Harisankar, A.H., c Raveendran, A., James, A., Latheef, B.A., Sankar, V., Noble, J. and Jarin, T., 2022, August. Intelligent robot for defect detection and rectification. In 2022 Third International Conference on Intelligent Computing Instrumentation and Control Technologies (ICICICT) (pp. 1753-1757). IEEE.

[8] Huang, P., Zhang, S., Li, M., Wang, J., Ma, C., Wang, B. and Lv, X., 2020. Classification of cervical biopsy images based on LASSO and EL-SVM. IEEE Access, 8, pp.24219-24228.

[9] Lee, S.A., Cho, H.C. and Cho, H.C., 2021. A novel approach for increased convolutional neural network performance in gastric-cancer classification using endoscopic images. IEEE Access, 9, pp.51847-51854.

[10] Kosaraju, S.C., Hao, J., Koh, H.M. and Kang, M., 2020. Deep-Hipo: Multi-scale receptive field deep learning for histopathological image analysis. Methods, 179, pp.3-13.

[11] Igarashi, S., Sasaki, Y., Mikami, T., Sakuraba, H. and Fukuda, S., 2020. Anatomical classification of upper gastrointestinal organs under various image capture conditions using AlexNet. Computers in Biology and Medicine, 124, p.103950.
[12] Wang, L., Jiao, Y., Qiao, Y., Zeng, N. and Yu, R., 2020. A novel approach combined transfer learning and deep learning to predict TMB from histology image. Pattern Recognition Letters, 135, pp.244-248.
[13] Li, L., Chen, M., Zhou, Y., Wang, J. and Wang, D., 2020, December. Research of deep learning on gastric cancer diagnosis. In 2020 Cross Strait Radio Science & Wireless Technology Conference (CSRSWTC) (pp. 1-3). IEEE.
[14] Wang, W., Tian, J., Zhang, C., Luo, Y., Wang, X. and Li, J., 2020. An improved deep learning approach and its applications on colonic polyp image detection. BMC Medical Imaging, 20, pp.1-14.
[15] Sun, R.J., Fang, M.J., Tang, L., Li, X.T., Lu, Q.Y., Dong, D., Tian, J. and Sun, Y.S., 2020. CT-based deep learning radiomics analysis for evaluation of serosa invasion in advanced gastric cancer. European Journal of Radiology, 132, p.109277.
[16] Ding, S., Huang, H., Li, Z., Liu, X. and Yang, S., 2020. SCNET: A novel UGI cancer screening framework based on semantic-level multimodal data fusion. IEEE journal of Biomedical and Health Informatics, 25(1), pp.143-151.
[17] Gamara, R.P.C., Loresco, P.J.M. and Bandala, A.A., 2022, December. Medical Chest X-ray Image Enhancement Based on CLAHE and Wiener Filter for Deep Learning Data Preprocessing. In 2022 IEEE 14th International Conference on Humanoid, Nanotechnology, Information Technology, Communication and Control, Environment, and Management (HNICEM) (pp. 1-6). IEEE.
[18] Borlea, I.D., Precup, R.E. and Borlea, A.B., 2022. Improvement of K-means cluster quality by post processing resulted clusters. Procedia Computer Science, 199, pp.63-70.
[19] Houssein, E.H., Çelik, E., Mahdy, M.A. and Ghoniem, R.M., 2022. Self-adaptive Equilibrium Optimizer for solving global, combinatorial, engineering, and Multi-Objective problems. Expert Systems with Applications, 195, p.116552.
[20] Premkumar, M., Jangir, P., Sowmya, R., Alhelou, H.H., Mirjalili, S. and Kumar, B.S., 2022. Multi-objective equilibrium optimizer: Framework and development for solving multi-objective optimization problems. Journal of Computational Design and Engineering, 9(1), pp.24-50.
[21] Hrosik, R.C., Tuba, E., Dolicanin, E., Jovanovic, R. and Tuba, M., 2019. Brain image segmentation based on firefly algorithm combined with k-means clustering. Stud. Inform. Control, 28(2), pp.167-176.
[22] PS, S.K. and Vs, D., 2016. Extraction of texture features using GLCM and shape features using connected regions. International journal of engineering and technology, 8(6), pp.2926-2930.
[23] Aggarwal, A.K., 2022. Learning texture features from glcm for classification of brain tumor mri images using random forest classifier. Transactions on Signal Processing, 18, pp.60-63.
[24] Zeidabadi, F.A. and Dehghani, M., 2022. POA: Puzzle Optimization Algorithm. International Journal of Intelligent Engineering & Systems, 15(1).
[25] Abualigah, L., Diabat, A., Mirjalili, S., Abd Elaziz, M. and Gandomi, A.H., 2021. The arithmetic optimization algorithm. Computer methods in applied mechanics and engineering, 376, p.113609.
[26] Hu, G., Zhong, J., Du, B. and Wei, G., 2022. An enhanced hybrid arithmetic optimization algorithm for engineering applications. Computer Methods in Applied Mechanics and Engineering, 394, p.114901.

[27] Wang, Z., Sacks, R. and Yeung, T., 2022. Exploring graph neural networks for semantic enrichment: Room type classification. Automation in Construction, 134, p.104039.
[28] Huang, Z., Tang, Y. and Chen, Y., 2022. A graph neural network-based node classification model on class-imbalanced graph data. Knowledge-Based Systems, 244, p.108538.
[29] Teramoto, A., Shibata, T., Yamada, H., Hirooka, Y., Saito, K. and Fujita, H., 2022. Detection and characterization of gastric cancer using cascade deep learning model in endoscopic images. Diagnostics, 12(8), p.1996.